

Article

Seismic Behavior of Steel-Fiber-Reinforced High-Strength Concrete Shear Wall with CFST Columns: Experimental Investigation

Ke Shi ¹ , Mengyue Zhang ¹, Pengfei Li ¹, Ru Xue ¹, Peibo You ², Tao Zhang ^{1,*} and Baoyu Cui ¹

¹ School of Civil Engineering and Architecture, Zhengzhou University of Aeronautics, Zhengzhou 450046, China; shike@zua.edu.cn (K.S.); zhangmengyue@zua.edu.cn (M.Z.); lipf2021@163.com (P.L.); xueru6239@163.com (R.X.); cuiyaoyu2021@163.com (B.C.)

² School of Civil and Transportation Engineering, Henan University of Urban Construction, Pingdingshan 467000, China; peiboyou2021@163.com

* Correspondence: zhangtao0226@zua.edu.cn

Abstract: To improve the seismic behavior of shear walls, a new composite shear wall composed of a steel-fiber-reinforced high-strength concrete (SFRHC) web and two square concrete-filled steel tube (CFST) columns, namely a steel-fiber-reinforced concrete shear wall with CFST columns, is proposed in this paper. Therefore, the main purpose of this paper is to present an experimental investigation of the seismic behavior of the SFRHC shear wall with CFST columns. Pseudo-static tests were carried out on seven composite shear walls, and the seismic performance of the shear walls was studied and quantified in terms of the aspects of energy consumption, ductility and stiffness degradation. Furthermore, the experimental results indicated that adding steel fiber can effectively restrain the crack propagation of composite shear walls and further help to improve the ductility and energy dissipation capacity of composite shear walls and delay the degradation of their lateral stiffness and force. Moreover, the seismic behavior of the SFRHC shear wall with CFST columns was obviously superior to that of the conventionally reinforced shear wall, in terms of load-bearing capacity, ductility, stiffness and energy dissipation capacity, because of the confinement effect of the CFST columns on the web. Finally, the preliminary study demonstrated that the composite shear wall has good potential to be used in regions with high seismic risk.

Keywords: composite shear wall; steel-fiber-reinforced high-strength concrete; square concrete-filled steel tubes; seismic behavior; load-bearing capacity



Citation: Shi, K.; Zhang, M.; Li, P.; Xue, R.; You, P.; Zhang, T.; Cui, B. Seismic Behavior of Steel-Fiber-Reinforced High-Strength Concrete Shear Wall with CFST Columns: Experimental Investigation. *Fibers* **2021**, *9*, 75. <https://doi.org/10.3390/fib9110075>

Academic Editor: Martin J. D. Clift

Received: 28 September 2021

Accepted: 11 November 2021

Published: 22 November 2021

Publisher's Note: MDPI stays neutral with regard to jurisdictional claims in published maps and institutional affiliations.



Copyright: © 2021 by the authors. Licensee MDPI, Basel, Switzerland. This article is an open access article distributed under the terms and conditions of the Creative Commons Attribution (CC BY) license (<https://creativecommons.org/licenses/by/4.0/>).

1. Introduction

Reinforced concrete shear walls are the key vertical bearing and lateral force-resisting component in high-rise buildings, widely used in earthquake-prone areas [1–4]. Its seismic performance is directly related to the overall safety of buildings. The research on earthquake damage shows that the main reason for the serious damage or collapse of shear walls lies in their poor ductility and energy dissipation capacity [5,6]. In the current design code, the axial compression ratio of shear walls should be strictly limited to meet the ductility requirements and avoid brittle failure. Therefore, the wall is often very thick, which reduces the usable area of the building and increases the self-weight of the structure. On the other hand, the restrained edge members of ordinary reinforced concrete shear walls must be equipped with many stirrups to effectively restrain the concrete and prevent longitudinal reinforcement from buckling under compression [7]. However, dense reinforcement increases the cost and affects the construction quality [8,9].

In order to overcome the shortcomings of ordinary reinforced concrete (RC) shear walls, researchers have put forward various forms of composite shear walls and conducted a great deal of research on their seismic behavior [10–15]. Meghdadian [16,17],

Kizilarslan [18–20] and Hu et al. [21] studied the seismic performance of composite shear walls with steel plates. Shi [22] and Jiang [23] studied the performance of double-skin composite walls subjected to in-plane cyclic loading. Zhang [24,25] studied the seismic behavior of composite shear walls with high-strength steel bars under cyclic loading. Yan [26,27] studied the seismic performance of concrete-filled composite plate shear walls. Researchers have also explored the use of steel trusses [28,29] and steel–concrete–steel composite plates for further reinforcement [30,31].

Among all kinds of composite shear walls, concrete-filled steel tube (CFST) side column shear walls are particularly attractive because the boundary element of concrete-filled steel tubes can help to resist external loads and serve as an additional constraint to restrain concrete. Ren [32] studied a composite shear wall composed of a reinforced concrete wall web and two boundary columns filled with carbon-fiber-reinforced polymer concrete. The results showed that the seismic performance of shear walls with CFST boundary columns was better than that of ordinary shear walls. The proposed composite shear wall had similar bearing capacity to the shear wall with double-skin CFST columns, but it had better ductility and greater dissipation capacity. Yan [33] proposed a type of steel–concrete–steel sandwich composite shear wall with J-hook connectors and CFST columns. The test results showed that all the concrete-filled steel tubular columns with the boundary experienced bending failure. Zhou [34,35] proposed a precast concrete-encased high-strength concrete-filled steel tube composite shear wall with twin steel tube connections. The experimental results showed that the composite shear wall had better hysteretic behavior, ductility, stiffness degradation and energy dissipation capacity.

In the past several years, the application of steel-fiber-reinforced concrete (SFRC) has been found increasingly in practice. Some researchers have conducted tests on the seismic behavior of SFRC shear walls. Due to the excellent properties of SFRC, such as tensile strength, shear resistance and crack resistance, SFRC can significantly improve the seismic performance of shear walls and reduce the phenomenon of steel bar blockage. Moreover, the ductility, energy dissipation capacity and bearing capacity of SFRC shear walls increase with an increase in the steel fiber volume fraction. Smarzewski [36,37] studied hybrid fiber-reinforced high-performance concrete deep beams with and without openings. The results showed that the initial cracking load, ultimate bearing capacity, toughness and ductility were improved with an increase in hybrid fiber content. Lim [38], Kang [39] and Choun [40] carried out cyclic loading tests on SFRC shear walls. The experimental results indicated that the seismic performance of the shear wall was obviously improved by adding steel fiber. Wei [41] studied the compression behavior of ultra-high-performance reinforced concrete columns confined by round steel tubes. The results demonstrated that the strength and ductility of the circular steel tube columns with steel fibers were greatly improved. Xu [42] investigated the seismic behavior of ultra-high-performance steel-fiber-reinforced concrete thin-walled steel tube columns under cyclic loading. The cyclic performance of the ultra-high-performance steel-fiber-reinforced concrete thin-walled steel tube columns was obviously better than that of ordinary-strength concrete-filled steel tube columns. Similarly, Lu [43] experimentally investigated the seismic behavior of steel-fiber-reinforced high-strength concrete (SFRHC) composite shear walls with different steel fiber volume fractions.

To sum up, previous research has mainly focused on concrete-filled steel tube shear walls or steel-fiber-reinforced concrete shear walls, with very little research on SFRHC shear walls with CFST columns. Therefore, this paper is devoted to exploring the seismic performance of composite shear walls by adding steel fibers with different volume fractions into square steel tubes by conducting experiments. The main parameters of the specimen include the steel fiber volume fraction, frame style, axial compression ratio and shear span ratio. Then, the failure characteristics, hysteretic curves, load-carrying capacity, stiffness degradation, energy dissipation capacity and deformation capacity of the specimens are discussed and studied in detail.

2. Experimental Program

2.1. Test Specimens and Materials

In accordance with the Chinese GB 50010-2010 [44] and GB 50936-2014 [45] standards, a total of 7 specimens were designed in this paper, including 1 ordinary RHC shear wall without CFST columns and 6 SFRHC shear walls with two CFST columns. The details of all specimens are summarized in Table 1, where the parameters mainly include the frame style (with or without CFST columns), steel fiber volume fraction (0, 0.5%, 1.0% and 1.5%), axial compression ratio (0.1 and 0.2) and shear span ratio (1.0 and 1.5).

Table 1. Detailed parameters of the test specimens.

Joint Number	Web Concrete Type	Dimension (mm × mm × mm)		Steel Fiber Volume Fraction (%)	Axial Compression Ratio	Shear Span Ratio
		Wall Web	Steel Tube			
RHC-0	C60	975 × 750 × 120	–	0	0.2	1.5
CFST-1	C60	975 × 750 × 120	120 × 120 × 3	0	0.2	1.5
CFST-2	CF60	975 × 750 × 120	120 × 120 × 3	0.5	0.2	1.5
CFST-3	CF60	975 × 750 × 120	120 × 120 × 3	1.0	0.2	1.5
CFST-4	CF60	975 × 750 × 120	120 × 120 × 3	1.5	0.2	1.5
CFST-5	CF60	975 × 750 × 120	120 × 120 × 3	1.0	0.1	1.5
CFST-6	CF60	600 × 750 × 120	120 × 120 × 3	1.0	0.2	1.0

Note: C stands for normal concrete; CF stands for steel-fiber-reinforced concrete.

The configurations and reinforcing details of the specimens with a shear span ratio of 1.5 are shown in detail in Figure 1, where the web height of the composite shear walls is 975 mm, and the cross-section is 750 mm × 120 mm (Figure 1a). Two CFST columns with the same side length of 120 mm and thickness of 3 mm were installed in the composite shear wall (Figure 1b). In addition, to fix the wall and apply the load, a foundation beam with a cross-section of 450 × 500 mm² and a top beam with a cross-section of 250 × 300 mm² were designed. To ensure reliable connections between the CFST columns and the shear wall web, U-shaped connectors [46] were also welded to the steel tubes (Figure 1e). The web height of the CFST-6 specimen was 600mm, while the other parameters were kept the same as the test specimens mentioned above.

2.2. Materials

Two kinds of concrete (RHC (C60) and SFRHC (CF60)) were poured into the wall webs, as shown in Table 1. It is worth noting that C60 was used to cast the foundation beam, top beam and CFST columns. Ordinary Portland cement and clean tap water were used in the experiment. Coarse aggregate and fine aggregate were selected from gravel with a continuous grain size of 5–20 mm and natural river sand, respectively. Uniform distribution of steel fiber is the key to preparing steel-fiber-reinforced concrete. To avoid the agglomeration of steel fiber, a forced mixer was selected for mixing. Firstly, all the dried mixed crushed stone, sand and steel fiber were added to the cement and high-range water-reducing admixture and mixed evenly. Then, water was injected while stirring. The steel fibers were used to form a hook shape, with an aspect ratio of $l_f/d_f = 35 \text{ mm}/0.55 \text{ mm} = 64$ and tensile strength of 1345 MPa. The detailed composition of the concrete is listed in Table 2.

For each type of steel-fiber-reinforced concrete, four groups of cube specimens and two groups of hexagonal prism specimens were prepared and cured under the same conditions. Then, a material test was conducted to obtain the cube compressive strength after curing for 28 days and on the day of the formal test, respectively. On the day of the test, two groups of prismatic specimens were used to measure the compressive strength and elastic modulus of the concrete. The material test results measured according to Chinese standard GB/T50081-2002 [47,48] are listed in Table 2.

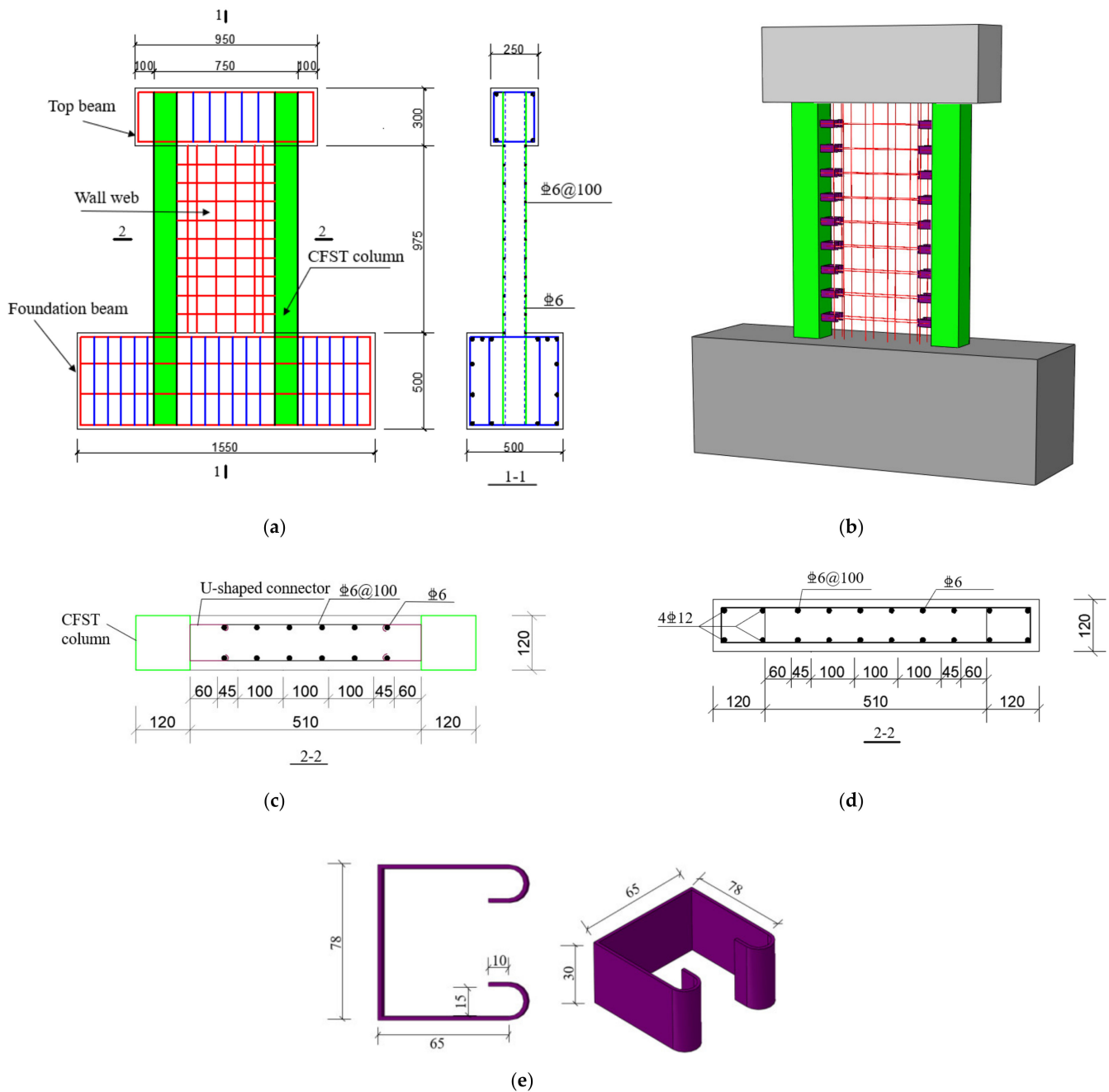


Figure 1. Dimensions and reinforcing details of the specimens. (a) Reinforcements of the specimens with CFST columns; (b) Solid diagram of the specimens; (c) Cross-section of the CFST specimens; (d) Cross-section of the RHC-0 specimen; (e) Dimensions of U-shaped connector (unit: mm).

Finally, the thicknesses of the CFST columns and U-shaped connectors were 3 mm and 2 mm, respectively, and they were composed of cold-formed steel tubes. The strength grade of the reinforcing bar and steel plate was HRB400 and Q235B, respectively, according to the Chinese GB/T228-2002 standard [49]. Table 3 presents the material properties of the steel plate and reinforcing bar.

Table 2. Mix proportion and mechanical properties of concrete.

Concrete Type	Steel Fiber Volume Fraction (%)	Mix Proportion (kg/m ³)					f_c (MPa)	f_t (MPa)	Modulus of Elasticity (Mpa)	
		Steel Fiber	Water	Cement	Sand	Stone				Water Reducer
C60	0	0.0	164	529	646	1110	5.819	55.3	2.8	41,500
CF60	0.5%	39	164	529	646	1110	5.819	55.5	3.7	41,600
CF60	1.0%	78	164	529	646	1110	5.819	55.9	6.2	42,100
CF60	1.5%	117	164	529	646	1110	5.819	56.8	7.9	42,300

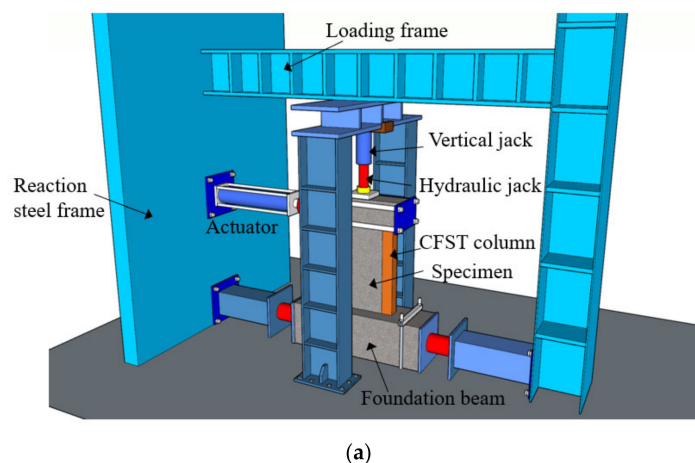
Table 3. Material properties of steel plate and bar.

Category	Yield Strength f_y (MPa)	Ultimate Strength f_u (Mpa)	Elastic Modulus (Mpa)
C6	369.2	521.6	185,000
2 mm plate	236.67	323.20	188,000
3 mm plate	307.07	392.20	198,000

2.3. Experimental Device and Loading System

The test loading device is shown in Figure 2. Firstly, the shear wall specimen was placed in the vertical reaction frame of the test loading system, and then the foundation beam of the specimen was fixed to the rigid floor with anchor bolts and horizontal compression beams. The vertical axial force was applied by a hydraulic jack of 2000 kN. The upper end of the hydraulic jack was connected with the vertical reaction frame through rolling support to ensure that the vertical axial force could move synchronously when the shear wall specimen moved horizontally. The lower end of the hydraulic jack was a rigid distribution beam with high rigidity to ensure that the vertical axial force could be uniformly applied to the wall. A horizontal cyclic load was applied by an electro-hydraulic servo-hydraulic actuator.

All shear wall specimens were subjected to horizontal low-cyclic loading under constant axial force. After the test began, a corresponding axial load was exerted on the loading beam and then loaded horizontally. Horizontal loading was controlled by displacement, and the loading system is shown in Figure 3. The displacement was expressed as the drift ratio θ , which is defined as the ratio of the lateral displacement at the loading point (Δ) to the height of the loading point above the wall base (H). The yield drift ratio θ_{ym} was designated as 1/400 according to the research in the literature [50]. Before the yield drift ratio θ_{ym} , the rotation levels of $0.5 \theta_{ym}$ and $0.75 \theta_{ym}$ were imposed. After the yield drift ratio θ_{ym} , three loading cycles were repeated at each drift level according to $10\theta_{ym}$, $20\theta_{ym}$, $30\theta_{ym}$ and so on. When the axial force could not be maintained or the lateral force degraded below 85% of the peak lateral force, the test was stopped.

**Figure 2.** Cont.



(b)

Figure 2. Experimental setup: (a) Schematic diagram; (b) Photo.

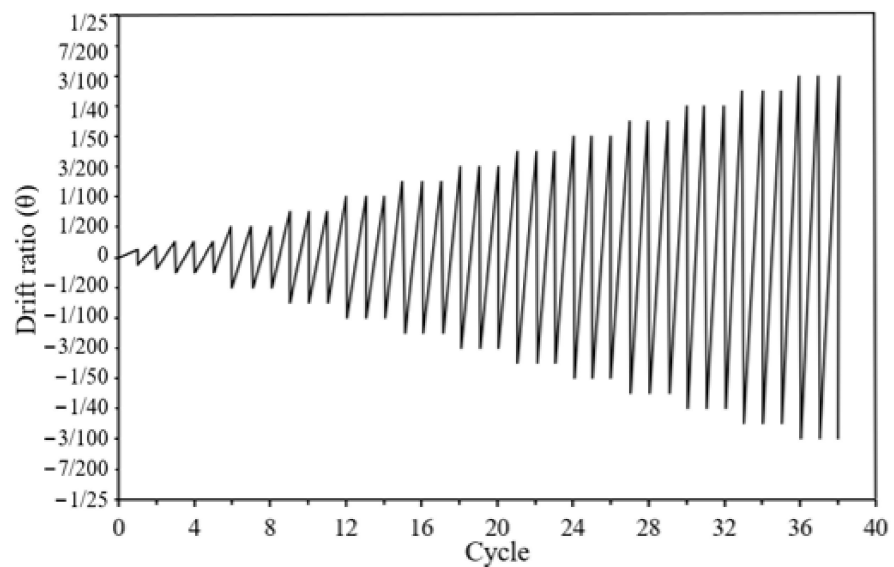


Figure 3. Loading history.

3. Test Results and Discussion

To better understand the seismic performance of the SFRHC shear wall with CFST columns, the effects of some key parameters on the behavior of the specimens are discussed and clarified in detail in this section, in terms of failure mode, hysteretic behavior, ductility, stiffness degradation and energy dissipation capacity.

3.1. Failure Modes

The loading program described in the previous section was conducted on all specimens, and the failure modes of the specimens at yield, peak point and failure point were recorded, respectively. Three keys are defined in the 'skeleton curves' section. Figure 4 shows the failure process of all specimens, and Figure 5 gives the failure modes of all the tested specimens. From Figures 4 and 5, it can be found that: (1) at the yield point (Y point), inclined cracks of nearly 45° developing obliquely downward in the wall webs were observed; in addition, the paint for CFST-series specimens was peeling at the column feet of the steel tubes on both sides, but to different extents; (2) as the force increased to the maximum value (P point), the distribution pattern of cracks remained unchanged, and

the width and number of cracks appreciably increased compared with the yield point Y; concrete spalling at the column-foot-restrained edge of specimen RHC-0 was serious; obvious outward bulges of the steel tubes on both sides of CFST-series specimens were observed; at the same time, there was concrete spalling in the wall webs in the middle of the CFST-1 and CFST-2 specimens; (3) when the force was reduced to 85% of the peak value, the specimen reached the ultimate state (point U), and the bearing capacity of the specimen decreased obviously; the concrete at the column-foot-restrained edge of the RHC-0 specimen was seriously peeled off; the buckling degree of the steel tubes on both sides of the CFST-series specimens gradually increased until torn, and the concrete at the foot of the column peeled off. The concrete in the middle of the CFST-1 and CFST-2 specimens also displayed extensive spalling. In particular, the failure modes for most of the specimens mainly comprised bending failure.



Figure 4. The failure process of all specimens: (a) RHC-0; (b) CFST-1; (c) CFST-2; (d) CFST-3; (e) CFST-4; (f) CFST-5; (g) CFST-6.

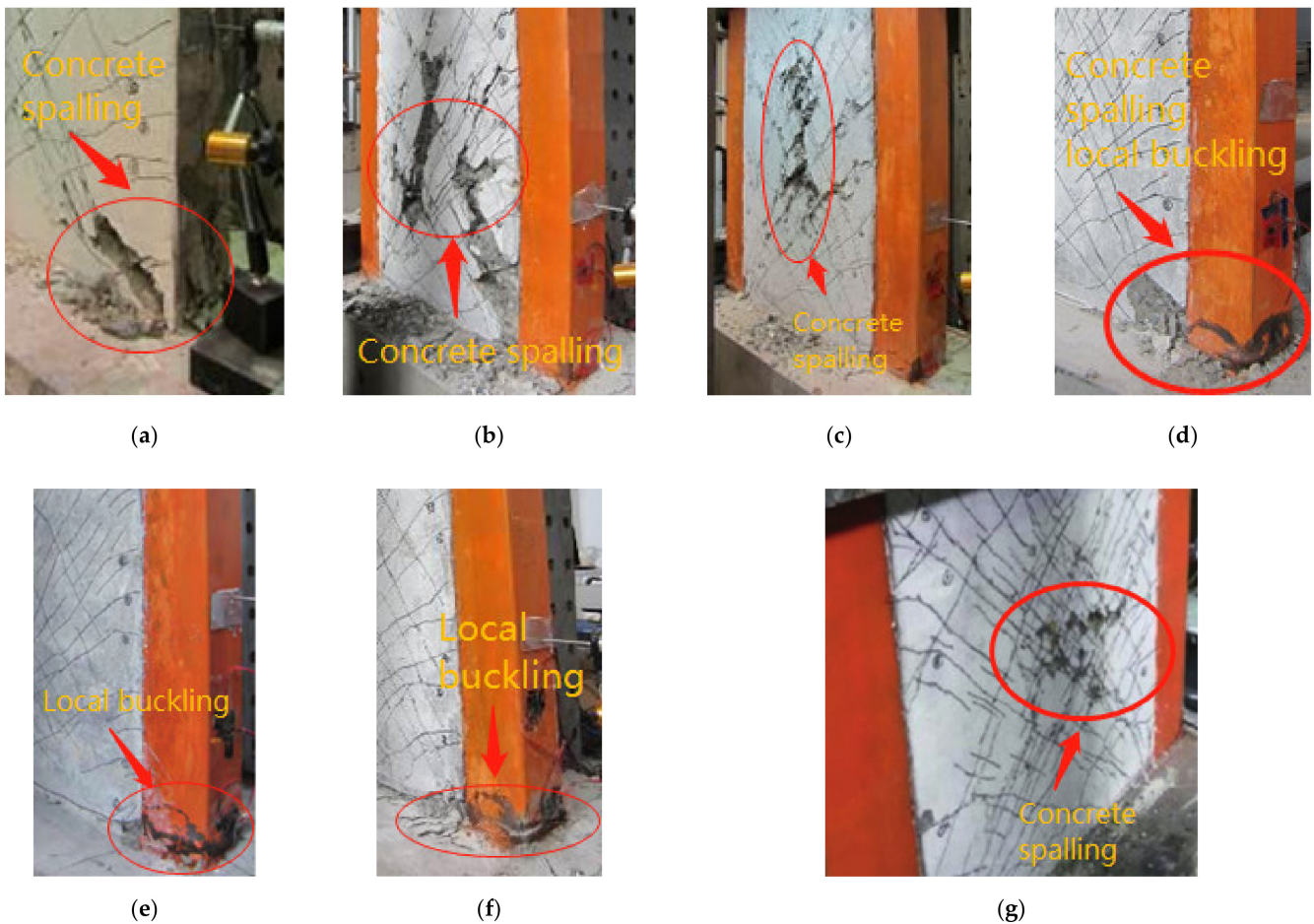


Figure 5. Failure patterns of shear wall specimens after test: (a) RHC-0; (b) CFST-1; (c) CFST-2; (d) CFST-3; (e) CFST-4; (f) CFST-5; (g) CFST-6.

Compared to the RHC-0 specimen, the CFST-1 specimen was relatively slow to produce cracks, and the crack width was also reduced. Both RHC-0 and CFST-1 specimens were subjected to bending and shear failure. The main crack widths of RHC-0 and CFST-1 were 2.54 mm and 1.82 mm, respectively. In comparison to the RHC-0 specimen, the main crack width of the CFST-1 specimen was reduced by 28.3%. The main reason for this was that the confinement effect of the CFST columns to the wall webs was stronger than that of the reinforced concrete side columns.

With the increase in the steel fiber volume fraction, the crack formation and development tended to slow down. Under the peak force, with a steel fiber volume fraction of 0%, 0.5%, 1.0% and 1.5%, the main crack widths of the CFST-1, CFST-2, CFST-3 and CFST-4 specimens were 1.82 mm, 1.25 mm, 1.07 mm and 0.84 mm, respectively. Compared to specimen CFST-1, the main crack widths of the CFST-2, CFST-3 and CFST-4 specimens were decreased by 31.3%, 41.2% and 53.8%, respectively. This was mainly due to the effective bonding between the steel fiber and concrete, which could improve the overall bearing capacity of the specimens and effectively delay the cracking process of shear wall specimens. At the same time, after the specimen cracked, the steel fiber running through both sides of the crack still needed to consume a great deal of energy in the process of pulling out, which inhibited the development of the crack width. It could be seen that steel fiber was able to significantly improve the shape of the cracks, and the cracks in the wall were generally thin and dense, limiting the width of the main cracks and alleviating the crushing and spalling of the concrete. In addition, CFST-2, CFST-3 and CFST-4 specimens

all suffered from bending failure, indicating that the addition of steel fiber can change the failure mode of shear walls.

Compared to the CFST-3 specimen, the failure rate of the CFST-5 specimen increased, and the failure degree of the steel tubes decreased. However, the failure characteristics of the two specimens and the distribution of cracks in the wall concrete were essentially the same.

With the increase in the shear span ratio from 1.0 to 1.5, the failure mode changed from shear failure to flexural failure. The specimens with a shear span ratio of 1.0 showed minor spalling on the wall web surface, while the shear wall specimens with a shear span ratio of 1.5 showed concrete spalling at the column foot.

3.2. Hysteretic Curve

The lateral force vs. lateral displacement hysteretic curves for all tested specimens are given in Figure 6. At the initial stage of the load, the load increased linearly with the increase in the displacement, indicating that the composite shear walls were in the elastic phase. In other words, no residual deformation occurred at the loading point. With the increase in the applied displacement, the area of the hysteresis loop became larger. Immediately after the vertical cracks formed in the wall web, the stiffness of the hysteretic curve decreased slightly and the strength increased steadily. Obvious residual deformation could be observed when the lateral force returned to zero. These curves were pinched slightly to form an arch. With the further development of concrete cracks and continuous yielding of longitudinal reinforcement in the tensile zone, the specimens gradually yielded, and the hysteretic curve became an inverted S shape with an evident pinch. After reaching the peak force, the residual deformation became more apparent. Due to the crushing and spalling of concrete and the tearing of the steel pipes, the stiffness and strength decreased significantly. Under the same displacement level, with the increase in the number of cycles, the bearing capacity tended to decrease obviously. At the final failure, the hysteretic curve of the specimen was between the inverted S shape and the Z shape.

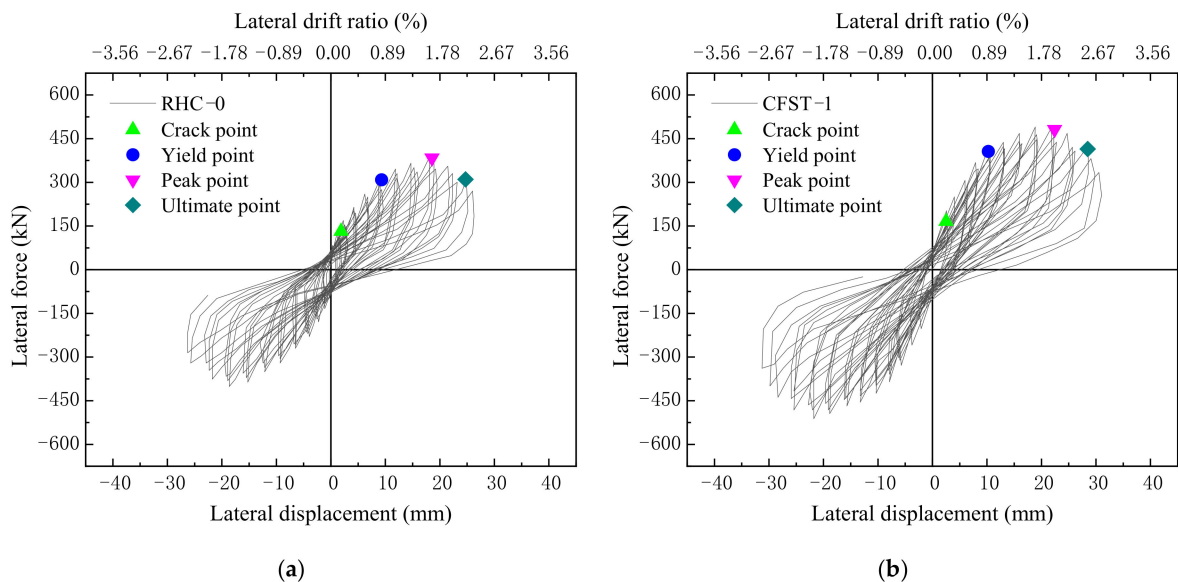


Figure 6. Cont.

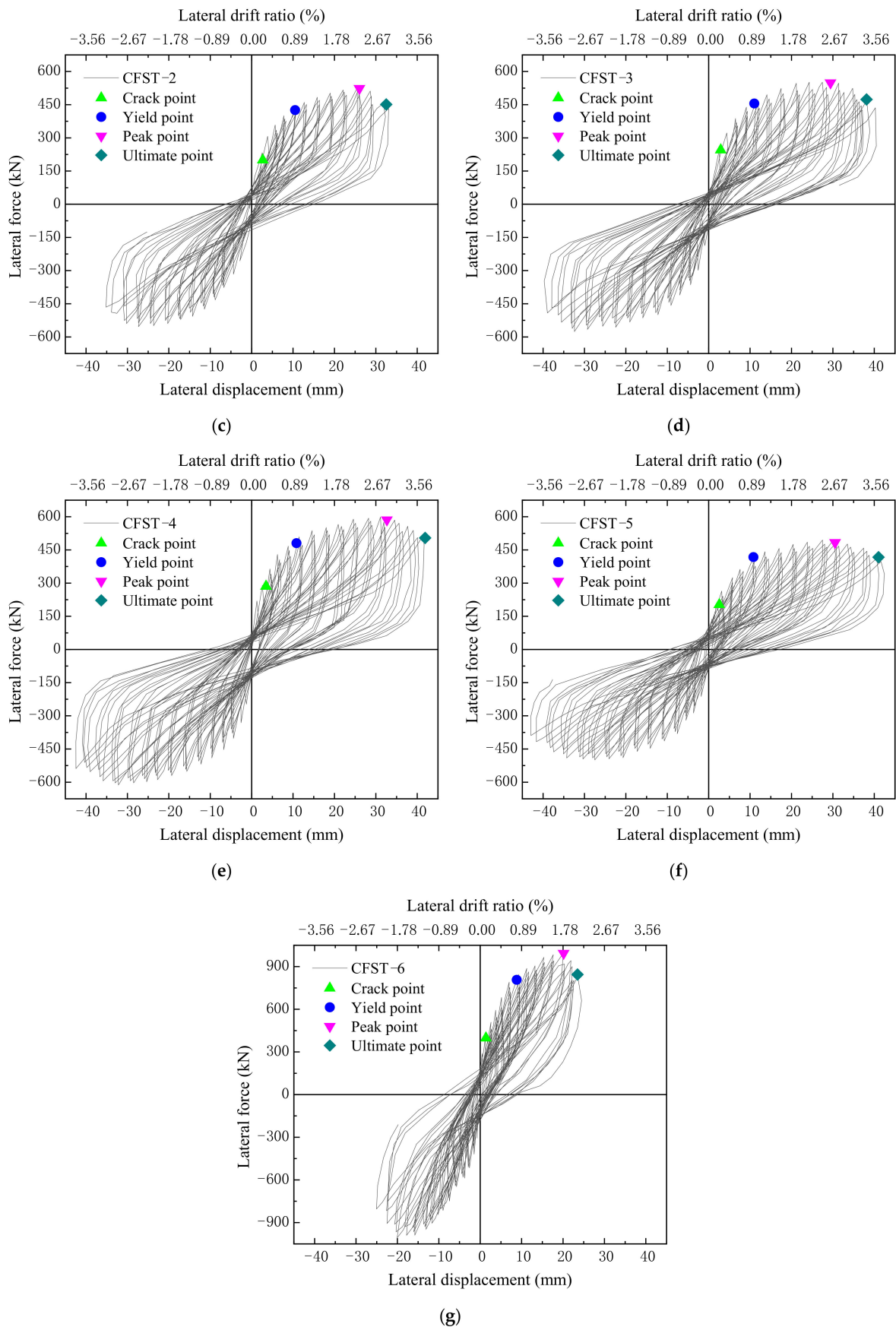


Figure 6. The hysteretic curves: (a) RHC-0; (b) CFST-1; (c) CFST-2; (d) CFST-3; (e) CFST-4; (f) CFST-5; (g) CFST-6.

Comparative analysis of the hysteretic curves for the RHC-0 and CFST-1 specimens showed that the elastic–plastic deformation and bearing capacity of the composite shear wall were improved, as a result of the confinement effect of the CFST columns on the shear walls. The peak force and displacement of the CFST-1 specimen were increased by 26% and 21% compared with the RHC-0 specimen. This was mainly due to the better restraint effect of the CFST-1 confined frame on the wall compared to the RHC-0 confined frame. On the one hand, this shows the reliable confinement effect of steel tubes on the core concrete. At the same time, the concrete in the steel tube can effectively prevent local damage caused by the concave shape, thus improving the bearing capacity of shear wall specimens. On the other hand, the effective connection between the concrete-filled steel tubular frame column and the middle wall causes the concrete-filled steel tubular frame column to mainly bear the bending action of the specimen. The shear wall panel mainly bore the shear action, which could cause the two to demonstrate better synergy.

With the increase in the steel fiber volume fraction, the elastic–plastic deformation, bearing capacity and hysteresis loop area of each hysteretic curve further increased, as shown in Figure 6. Compared to the CFST-1 specimen, the peak forces of CFST-2, CFST-3 and CFST-4 specimens were increased by 16%, 31% and 46%, respectively, and the peak displacements were increased by 9%, 14% and 22%, respectively. The experimental results showed that increasing the volume ratio of steel fiber can improve the bearing capacity of the wall and enhance the elastic–plastic deformation and energy dissipation capacity of the wall.

With the increase in the axial compression ratio, compared to the CFST-5 specimen, the peak force of the CFST-3 specimen was increased by 14%, and the peak displacement was decreased by 4%. The hysteresis loop areas of the two specimens were approximately equal, which indicates that the axial compression ratio had little effect on the energy consumption of the specimens.

As the shear span ratio increased from 1.0 to 1.5, the peak force of the CFST-3 specimen was decreased by 45% and the peak displacement was increased by 46% compared with the CFST-6 specimen. At the same time, the former showed a significant pinching effect.

3.3. Skeleton Curve

By connecting the peak points of each loading increment in sequence on the hysteresis curve, lateral force versus lateral displacement skeleton curves of the specimens could be obtained, as shown in Figure 7. The effects of the frame type, steel fiber volume ratio, axial compression ratio and shear span ratio on the bearing capacity and elastic stiffness of specimens can be clearly observed. In the elastic stage, the force and displacement were linear. After cracking, the curve had an obvious turning point, showing stiffness degradation. With the increase in displacement, the force increased further until the peak point was reached. After this, the curve suddenly dropped as the specimen was tested to failure. Table 4 lists the strength and displacement at different characteristic points. F_y and Δ_y (yield displacement) were determined using the energy equivalence method [51], as shown in Figure 8.

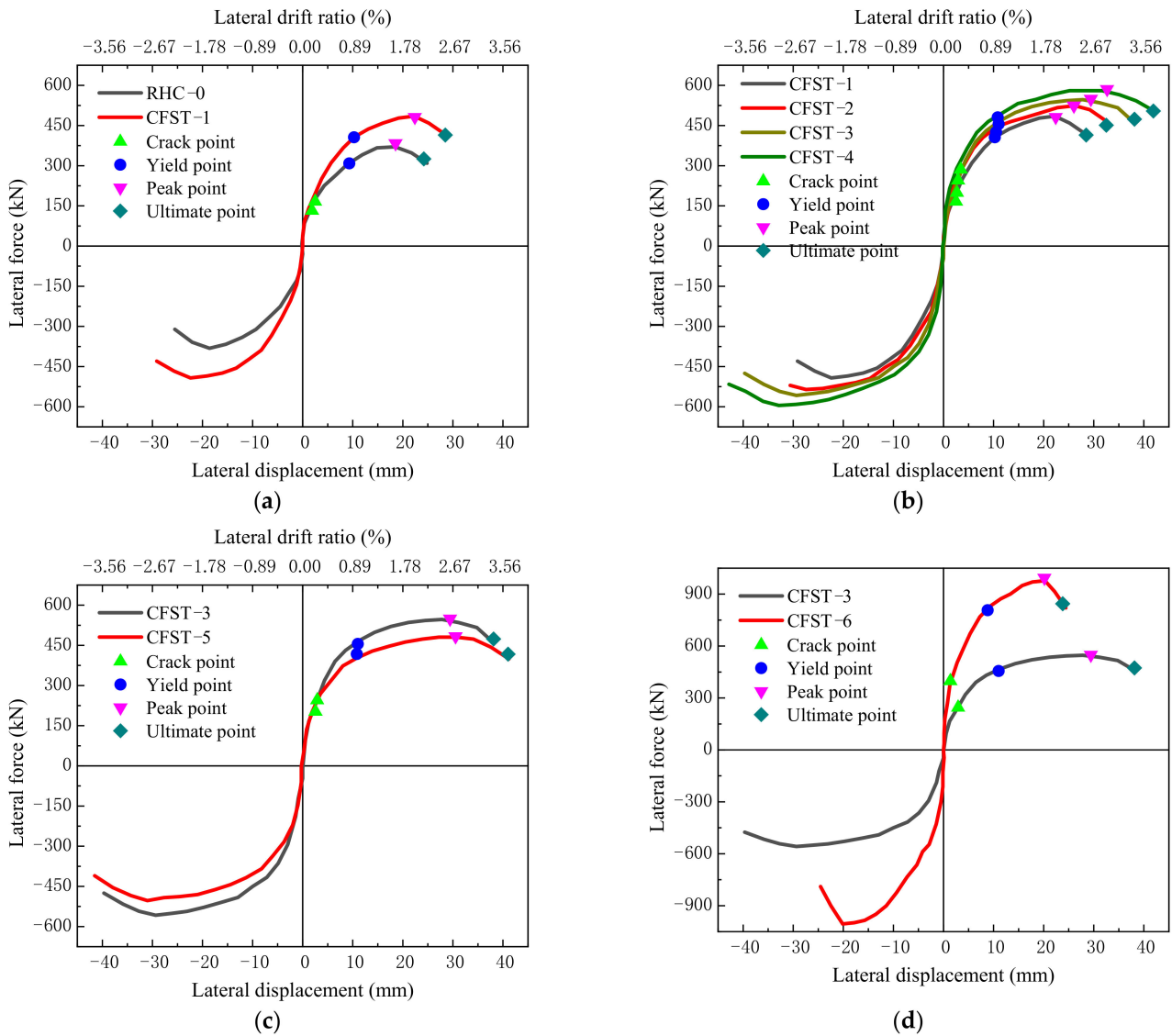


Figure 7. Skeleton curves of test specimens with (a) different frame style; (b) different steel fiber volume fraction; (c) different axial compression ratio; (d) different shear span ratio.

Table 4. Strength and displacement at different characteristic points.

Joint Number	Cracking Point		Yield Point		Peak Point		Ultimate Point		μ	E_{total}
	F_{cr} (kN)	Δ_y (mm)	F_y (kN)	Δ_y (mm)	F_m (kN)	Δ_m (mm)	F_u (kN)	Δ_u (mm)		
RHC-0	132.22	1.86	308.52	9.32	383.71	18.56	325.37	24.2	2.60	65.09
CFST-1	166.27	2.51	405.89	10.27	481.76	22.41	414.42	28.48	2.77	108.06
CFST-2	199.72	2.69	425.65	10.51	523.73	26.03	451.19	32.5	3.09	154.96
CFST-3	245.56	2.92	455.53	11.01	548.95	29.42	473.53	38.13	3.46	194.92
CFST-4	285.59	3.47	480.54	10.84	585.95	32.67	504.27	41.9	3.87	289.42
CFST-5	202.29	2.56	417.62	10.81	483.13	30.54	417.14	41.02	3.79	191.34
CFST-6	398.32	1.38	807.17	8.82	993.36	20.15	844.68	23.5	2.66	157.9

Note: F_{cr} is crack force. Δ_{cr} is crack displacement. F_y is yield force. Δ_y is yield displacement. F_m is peak force. Δ_m is peak displacement. F_u is ultimate force. Δ_u is ultimate displacement. μ is the ductility coefficient. E_{total} is accumulative energy dissipation.

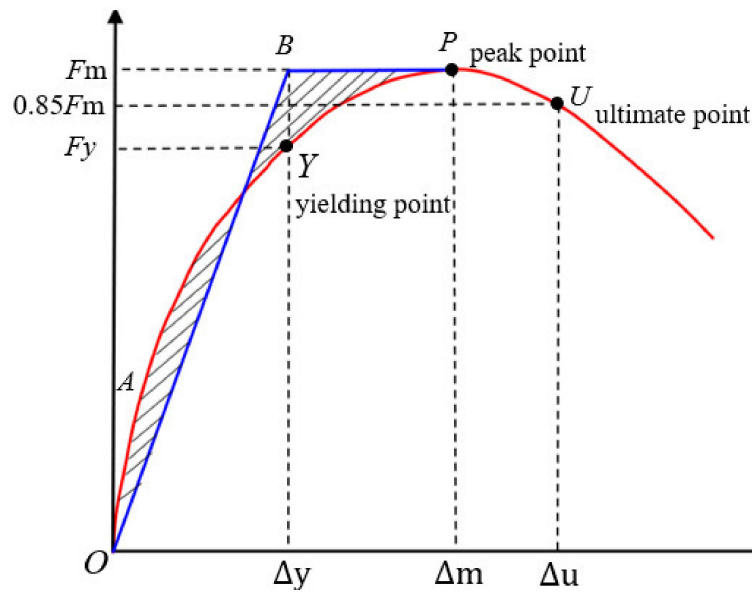


Figure 8. The method to determine yield point.

Figure 7a compares the skeleton curves of specimens with different frame styles. Compared to the RHC-0 specimen, the CFST-1 specimen had a larger envelope. In addition, the slope of the CFST-1 specimen's curve was larger than that of the RHC-0 curve at the initial loading stage, which indicates that the initial stiffness of the CFST shear wall was larger than that of the RHC curve.

Figure 7b presents the skeleton curves of specimens with different steel fiber volume fractions. Compared to specimen CFST-1, the crack force (F_{cr}) of CFST-2, CFST-3 and CFST-4 specimens with 0.5%, 1.0% and 1.5% steel fiber volume fractions was improved by 20%, 48% and 72%, respectively. The Δ_{cr} , Δ_y , Δ_m , Δ_u and corresponding forces increased significantly. This indicated that increasing the steel fiber volume fraction in the wall web was beneficial to delay the concrete cracking and improve the load-bearing capacity and deformation capacity. A higher steel fiber volume fraction usually leads to a greater improvement.

Figure 7c gives the skeleton curves of specimens with different axial compression ratios. The two specimens show similar initial stiffness. Compared with the CFST-5 specimen, the cracking force and yield force of CFST-3 were increased by 21% and 9%, and the corresponding cracking displacement and yield displacement were increased by 14% and 2%.

Figure 7d shows the skeleton curves of specimens with different shear span ratios. Compared to the CFST-6 specimen, the cracking force and yield force of the CFST-3 specimen were decreased by 38% and 44%, while the corresponding cracking displacement and yield displacement were increased by 112% and 25%. Moreover, the skeleton curve of the CFST-6 specimen rose sharply, and the bearing capacity dropped rapidly after reaching the peak value, indicating that its stiffness decayed rapidly after reaching the peak force.

3.4. Ductility Coefficient and Energy Dissipation

The energy dissipation capacity of specimens can be measured by the area of their lateral force vs. lateral displacement envelope. Deformation capacity is an important index of the seismic performance of composite shear walls, which is defined as the displacement ductility coefficient μ .

$$\mu = \frac{\Delta_u}{\Delta_y} \quad (1)$$

where Δ_u is the ultimate displacement and Δ_y is the yield displacement. The calculated values of the total energy dissipation (E_{total}) and ductility coefficient for each test are presented in Table 4 and Figures 9 and 10.

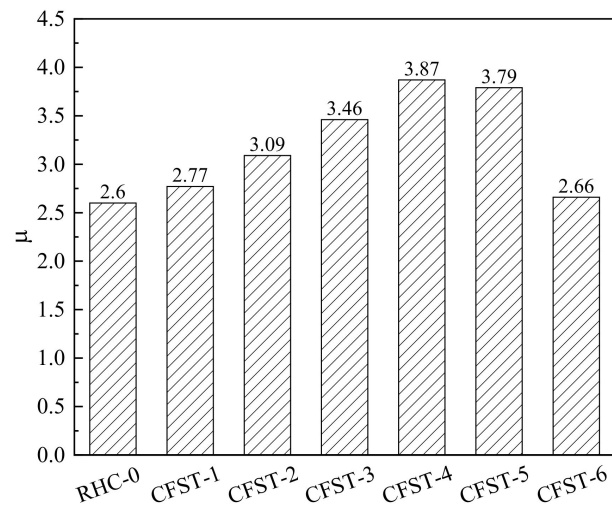


Figure 9. The ductility coefficient.

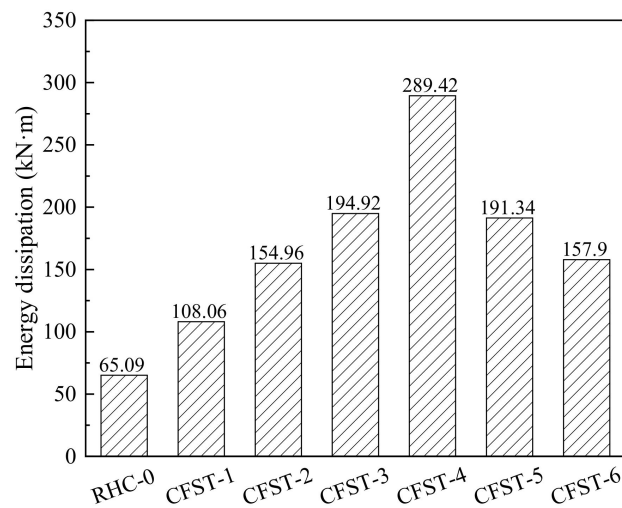


Figure 10. The energy dissipation.

In comparison to specimen RHC-0, the ductility coefficient and energy dissipation of the CFST-1 specimen were improved by 7%, and 66%, respectively. In addition, compared to the CFST-1 specimen, the ductility coefficients of CFST-2, CFST-3 and CFST-4 specimens were improved by 8.83%, 14.17% and 21.77%, respectively, and the energy dissipation was improved by 43%, 80% and 168%, with the increase in the steel fiber volume fraction from 0 to 0.5%, 0.5% to 1% and 1% to 1.5%. The results indicated that adding steel fiber to concrete can significantly improve the ductility and energy dissipation of specimens. However, increasing the axial compression ratio has little effect on the energy dissipation and has a negative effect on the ductility of walls. As the axial compression ratio increased from 0.1 to 0.2, compared with the CFST-5 specimen, the energy dissipation of the CFST-3 specimen was increased by only 2% and the ductility coefficient was decreased by 9%. In comparison to the CFST-6 specimen, the ductility coefficient and energy dissipation of the CFST-3 specimen were improved by 30% and 23%, respectively. This shows that increasing the shear span ratio can effectively improve the ductility and energy dissipation of an SFRHC shear wall with CFST columns.

3.5. Stiffness Degradation

The secant stiffness was used to characterize the stiffness degradation of the specimens under various loadings, and it was calculated according to the Specification for Seismic Test Buildings in China [51].

$$K_i = \frac{|+F_i| + |-F_i|}{|+\Delta_i| + |-\Delta_i|} \quad (2)$$

where $+F_i$ and $-F_i$ are the peak forces in the positive and negative directions under the i th loading, respectively; $+\Delta_i$ and $-\Delta_i$ are the displacements corresponding to the peak force in the positive and negative directions under the i th loading, respectively.

The secant stiffness of specimens with different displacements is shown in Figure 9. It can be seen that the stiffness degradation trend of all specimens was very close. At first, the stiffness degradation was fast, but the stiffness degradation slowed down as the specimen entered the yield stage. When the specimens were close to failure, the stiffness difference between the specimens became the smallest. The secant stiffness of each specimen decreased with the increase in displacement.

Figure 11a shows the effect of the frame style on the stiffness degradation of the specimens. This indicates that the composite shear walls with CFST columns had higher stiffness than the RHC shear wall without CFST columns. The initial stiffness of the CFST-1 specimen was 1.1 times that of the RHC-0 specimen, and the stiffness degradation curve slowed down. This implies that the confinement effect of the CFST columns on the wall webs could effectively mitigate the stiffness degradation and increase the initial elastic stiffness of the shear wall specimens.

Figure 11b compares the effect of steel fiber volume fraction on the stiffness degradation of the specimens. With the increase in the steel fiber volume fraction, the stiffness degradation rate of SFRHC specimens was slightly slower than that of RHC specimens, especially in the crack development stage. The reason for this is that the steel fiber prevented crack propagation and improved the stress redistribution in the rapid crack development stage. Therefore, crack development was postponed and distributed more uniformly. Hence, the stiffness degradation rate decreased, and the impact of the steel fiber was gradually reduced.

Figure 11c shows the effect of the axial compression ratio on the stiffness degradation of specimens. The initial stiffness of CFST-3 and CFST-5 specimens was similar. However, in the later loading process, the stiffness degradation rate of the CFST-3 specimen was more significant.

Figure 11d presents the effect of the shear span ratio on the stiffness degradation of the specimens. When the shear span ratio increased from 1.0 to 1.5, the initial stiffness of the shear wall specimens decreased by 64%, but the stiffness degradation curve tended to slow down.

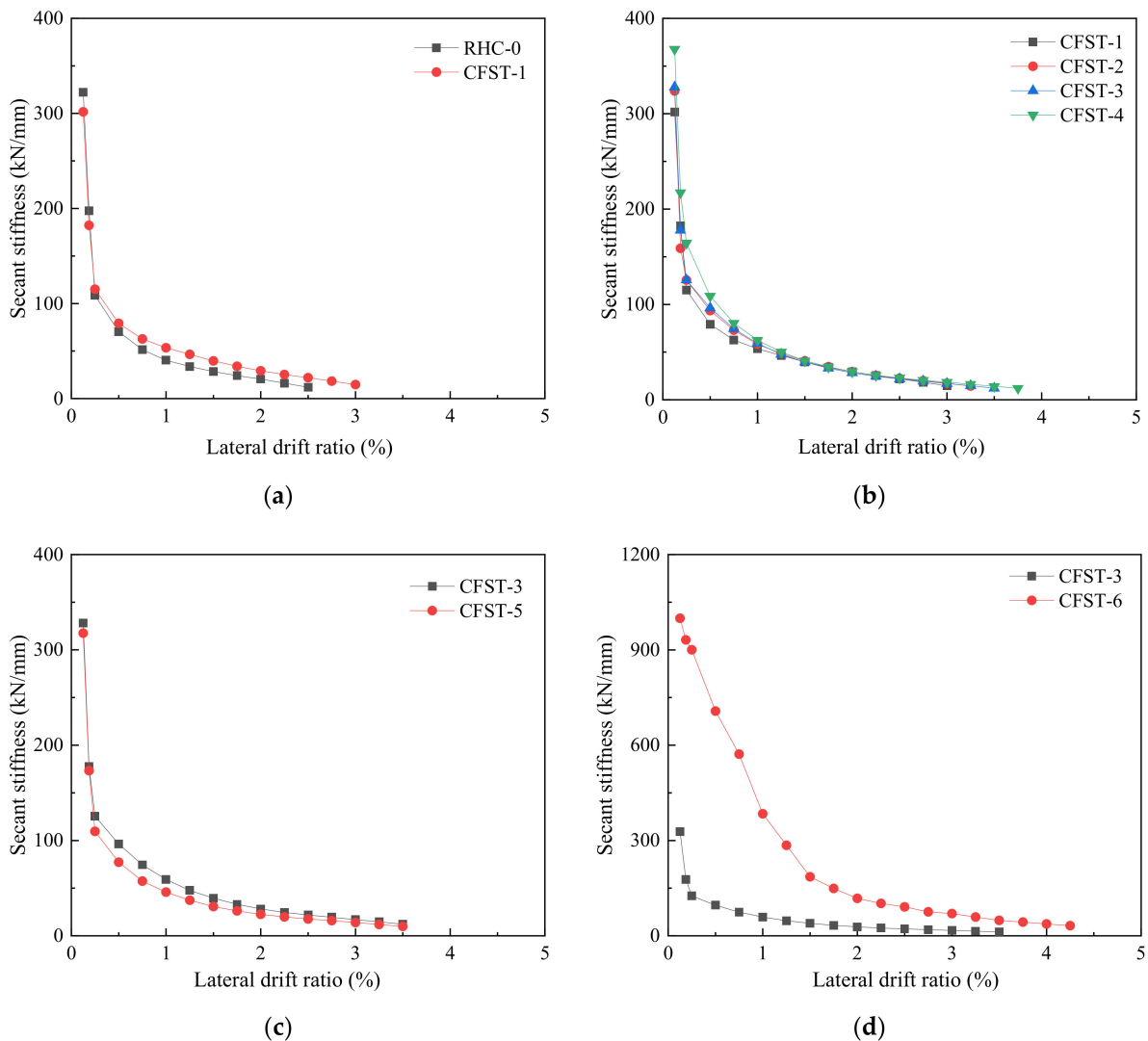


Figure 11. The stiffness degradation with (a) different frame style; (b) different steel fiber volume fraction; (c) different axial compression ratio; (d) different shear span ratio.

4. Conclusions

In this paper, the hysteretic behavior of SFRHC shear walls with CFST columns under cyclic loading was studied via experiments. The deformation, stiffness degradation and energy dissipation of specimens were discussed. Based on the experimental results of the current research, the main conclusions were drawn as follows:

- Compared to the ordinary shear wall, the cracking force, yielding force, peak force, deformation capacity, ductility and energy dissipation capacity of the composite shear wall were significantly improved; in particular, the energy dissipation capacity was increased by 66%. This demonstrated that CFST columns can significantly improve the seismic performance of SFRHC shear walls, due to the confinement effect on the shear web.
- With the addition of steel fiber, the energy dissipation capacity, ductility coefficient and load-bearing capacity of the specimens were increased. In addition, the failure mode of the shear wall changed from shear failure to bending failure due to the crack resistance of steel fiber.
- Comparative analysis of seismic performance between CFST-3 and CFST-5 specimens demonstrated that increasing the axial compression ratio of shear walls can increase the cracking force, yield force and peak force of specimens, and has little influence

on the energy consumption. However, it has a negative impact on the ductility of the specimens.

- Comparative analysis of seismic performance between CFST-3 and CFST-6 specimens illustrated that increasing the shear span ratio of shear walls can increase the ductility and energy dissipation of specimens. However, it decreased the cracking force, yield force and peak force (all >35%).

Author Contributions: Conceptualization and design, data curation, investigation, and resources, K.S.; data curation, writing—original draft preparation, and formal analysis, M.Z.; conceptualization, formal analysis, and writing—review and editing, T.Z.; visualization and project administration, R.X.; formal analysis, visualization, and methodology, P.Y.; data curation and formal analysis, P.L.; investigation and visualization, B.C. All authors have read and agreed to the published version of the manuscript.

Funding: This research was funded by the National Natural Science Foundation of China (51708514, 52108207), Key Scientific Research Projects of Colleges and Universities of Henan Provincial Department of Education (21A560015).

Institutional Review Board Statement: Not applicable.

Informed Consent Statement: Not applicable.

Data Availability Statement: Data are available on request from the authors.

Acknowledgments: The authors acknowledge the financial support of the National Natural Science Foundation of China (51708514, 52108207), Key Scientific Research Projects of Colleges and Universities of Henan Provincial Department of Education (21A560015).

Conflicts of Interest: The authors declare that they have no conflicts of interest.

References

1. Peng, Y.; Wu, H.; Zhuge, Y. Strength and drift capacity of squat recycled concrete shear walls under cyclic loading. *Eng. Struct.* **2015**, *100*, 356–368. [[CrossRef](#)]
2. Bekő, A.; Rosko, P.; Wenzel, H.; Pegon, P.; Markovic, D.; Molina, F.J. RC shear walls: Full-scale cyclic test, insights and derived analytical model. *Eng. Struct.* **2015**, *102*, 120–131. [[CrossRef](#)]
3. Li, B.; Qian, K.; Wu, H. Flange effects on seismic performance of reinforced concrete squat walls with irregular or regular openings. *Eng. Struct.* **2016**, *110*, 127–144. [[CrossRef](#)]
4. Mosoarca, M. Failure analysis of RC shear walls with staggered openings under seismic loads. *Eng. Fail. Anal.* **2014**, *41*, 48–64. [[CrossRef](#)]
5. Zhang, H.M.; Lu, X.L.; Duan, Y.F.; Zhu, Y. Experimental study on failure mechanism of RC walls with different boundary elements under vertical and lateral loads. *Adv. Struct. Eng.* **2014**, *17*, 361–379. [[CrossRef](#)]
6. Massone, L.M.; Wallace, J.W. Load-deformation responses of slender reinforced concrete walls. *Struct. J.* **2004**, *101*, 103–113.
7. Massone, L.M.; Bonelli, P.; Lagos, R.; Lüders, C.; Moehle, J.; Wallace, J.W. Seismic design and construction practices for RC structural wall buildings. *Earthq. Spectra* **2012**, *28*, 245–256. [[CrossRef](#)]
8. Sener, K.C.; Varma, A.H.; Ayhan, D. Steel-plate composite (SC) walls: Out-of-plane flexural behavior, database, and design. *J. Constr. Steel Res.* **2015**, *108*, 46–59. [[CrossRef](#)]
9. Seo, J.; Varma, A.H.; Sener, K.; Ayhan, D. Steel-plate composite (SC) walls: In-plane shear behavior, database, and design. *J. Constr. Steel Res.* **2016**, *119*, 202–215. [[CrossRef](#)]
10. Bogdanić, A.; Casucci, D.; Ožbolt, J. Numerical and experimental investigation of anchor channels subjected to shear load in composite slabs with profiled steel decking. *Eng. Struct.* **2021**, *240*, 112347. [[CrossRef](#)]
11. Cheng, S.; Yin, S.; Jing, L. Comparative experimental analysis on the in-plane shear performance of brick masonry walls strengthened with different fiber reinforced materials. *Constr. Build. Mater.* **2020**, *259*, 120387. [[CrossRef](#)]
12. Chu, Y.; Hou, H.; Yao, Y. Experimental study on shear performance of composite cold-formed ultra-thin-walled steel shear wall. *J. Constr. Steel Res.* **2020**, *172*, 106168. [[CrossRef](#)]
13. Hossain, K.M.A.; Jahan, A.; Mol, L. Experimental and analytical investigation on shear behavior of profiled steel sheet dry board composite wall system. *Structures* **2021**, *34*, 3945–3957. [[CrossRef](#)]
14. Kenarangi, H.; Kizilarlan, E.; Bruneau, M. Cyclic behavior of c-shaped composite plate shear walls—Concrete filled. *Eng. Struct.* **2021**, *226*, 111306. [[CrossRef](#)]
15. Xingxing, W.; Wei, W.; Jihong, Y.; Youcheng, L. Synergistic shear behaviour of cold-formed steel shear walls and reinforced edge struts. *J. Constr. Steel Res.* **2021**, *184*, 106779. [[CrossRef](#)]

16. Meghdadaian, M.; Ghalehnovi, M. Improving seismic performance of composite steel plate shear walls containing openings. *J. Build. Eng.* **2019**, *21*, 336–342. [[CrossRef](#)]
17. Meghdadian, M.; Gharaei-Moghaddam, N.; Arabshahi, A.; Mahdavi, N.; Ghalehnovi, M. Proposition of an equivalent reduced thickness for composite steel plate shear walls containing an opening. *J. Constr. Steel Res.* **2020**, *168*, 105985. [[CrossRef](#)]
18. Kizilarслан, E.; Broberg, M.; Shafaei, S.; Varma, A.H.; Bruneau, M. Non-linear analysis models for Composite Plate Shear Walls-Concrete Filled (C-PSW/CF). *J. Constr. Steel Res.* **2021**, *184*, 106803. [[CrossRef](#)]
19. Kizilarслан, E.; Broberg, M.; Shafaei, S.; Varma, A.H.; Bruneau, M. Seismic design coefficients and factors for coupled composite plate shear walls/concrete filled (CC-PSW/CF). *Eng. Struct.* **2021**, *244*, 112766. [[CrossRef](#)]
20. Kizilarслан, E.; Bruneau, M. Hysteretic behavior of repaired C-shaped concrete filled-composite plate shear walls (C-PSW/CF). *Eng. Struct.* **2021**, *241*, 112410. [[CrossRef](#)]
21. Hu, H.; Nie, J.; Fan, J.; Tao, M.; Wang, Y.; Li, S. Seismic behavior of CFST-enhanced steel plate-reinforced concrete shear walls. *J. Constr. Steel Res.* **2016**, *119*, 176–189. [[CrossRef](#)]
22. Shi, J.; Guo, L.; Qu, B. In-plane cyclic tests of double-skin composite walls with concrete-filled steel tube boundary elements. *Eng. Struct.* **2022**, *250*, 113301. [[CrossRef](#)]
23. Jiang, J.; Luo, J.; Xue, W.; Hu, X.; Qin, D. Seismic performance of precast concrete double skin shear walls with different vertical connection types. *Eng. Struct.* **2021**, *245*, 112911. [[CrossRef](#)]
24. Zhang, J.; Liu, J.; Li, X.; Cao, W. Seismic behavior of steel fiber-reinforced high-strength concrete mid-rise shear walls with high-strength steel rebar. *J. Build. Eng.* **2021**, *42*, 102462. [[CrossRef](#)]
25. Zhang, J.; Liu, J.; Zhang, D.; Huang, X. Hysteretic behavior of high-performance frame-shear wall composite structure with high-strength steel bars. *J. Build. Eng.* **2022**, *45*, 103416. [[CrossRef](#)]
26. Yan, J.; Hu, H.; Wang, T. Cyclic tests on concrete-filled composite plate shear walls with enhanced C-channels. *J. Constr. Steel Res.* **2021**, *179*, 106522. [[CrossRef](#)]
27. Yan, J.; Hu, H.; Wang, T. Seismic behaviour of novel concrete-filled composite plate shear walls with boundary columns. *J. Constr. Steel Res.* **2021**, *179*, 106507. [[CrossRef](#)]
28. Shi, J.; Gao, S.; Guo, L. Compressive behaviour of double skin composite shear walls stiffened with steel-bars trusses. *J. Constr. Steel Res.* **2021**, *180*, 106581. [[CrossRef](#)]
29. Xiong, M.; Xiong, D.; Liew, J.R. Flexural performance of concrete filled tubes with high tensile steel and ultra-high strength concrete. *J. Constr. Steel Res.* **2017**, *132*, 191–202. [[CrossRef](#)]
30. Huang, Z.; Liew, J.R. Structural behaviour of steel–concrete–steel sandwich composite wall subjected to compression and end moment. *Thin Wall Struct.* **2016**, *98*, 592–606. [[CrossRef](#)]
31. Chen, Z.; Zi, Z.; Zhou, T.; Wu, Y. Axial compression stability of thin double-steel-plate and concrete composite shear wall. *Structures* **2021**, *34*, 3866–3881. [[CrossRef](#)]
32. Ren, F.; Chen, J.; Chen, G.; Guo, Y.; Jiang, T. Seismic behavior of composite shear walls incorporating concrete-filled steel and FRP tubes as boundary elements. *Eng. Struct.* **2018**, *168*, 405–419. [[CrossRef](#)]
33. Yan, J.; Yan, Y.; Wang, T. Cyclic tests on novel steel-concrete-steel sandwich shear walls with boundary CFST columns. *J. Constr. Steel Res.* **2020**, *164*, 105760. [[CrossRef](#)]
34. Zhou, J.; Li, P.; Guo, N. Seismic performance assessment of a precast concrete-encased CFST composite wall with twin steel tube connections. *Eng. Struct.* **2020**, *207*, 110240. [[CrossRef](#)]
35. Zhou, J.; Fang, X.; Yao, Z. Mechanical behavior of a steel tube-confined high-strength concrete shear wall under combined tensile and shear loading. *Eng. Struct.* **2018**, *171*, 673–685. [[CrossRef](#)]
36. Smarzewski, P. Hybrid Fibres as Shear Reinforcement in High-Performance Concrete Beams with and without Openings. *Appl. Sci.* **2018**, *8*, 2070. [[CrossRef](#)]
37. Smarzewski, P. Analysis of Failure Mechanics in Hybrid Fibre-Reinforced High-Performance Concrete Deep Beams with and without Openings. *Materials* **2018**, *12*, 101. [[CrossRef](#)]
38. Lim, W.G.; Kang, S.W.; Yun, H.D. Shear Behavior of Squat Steel Fiber Reinforced Concrete (SFRC) Shear Walls with Vertical Slits. *Appl. Mech. Mater.* **2013**, *372*, 207–210. [[CrossRef](#)]
39. Eom, T.; Kang, S.; Kim, O. Earthquake resistance of structural walls confined by conventional tie hoops and steel fiber reinforced concrete. *Earthq. Struct.* **2014**, *7*, 843–859. [[CrossRef](#)]
40. Choun, Y.S.; Lee, J.H.; Jeon, J.K. Evaluation of Shear Resisting Capacity of a Conventional Reinforced Concrete Wall with Steel or Polyamide Fiber Reinforcement. *J. Korean Soc. Hazard Mitig.* **2013**, *13*, 1–7. [[CrossRef](#)]
41. Wei, J.; Xie, Z.; Zhang, W.; Luo, X.; Yang, Y.; Chen, B. Experimental study on circular steel tube-confined reinforced UHPC columns under axial loading. *Eng. Struct.* **2021**, *230*, 111599. [[CrossRef](#)]
42. Xu, S.; Wu, C.; Liu, Z.; Shao, R. Experimental investigation on the cyclic behaviors of ultra-high-performance steel fiber reinforced concrete filled thin-walled steel tubular columns. *Thin Wall. Struct.* **2019**, *140*, 1–20. [[CrossRef](#)]
43. Lu, X.; Zhang, Y.; Zhang, H.; Zhang, H.; Xiao, R. Experimental study on seismic performance of steel fiber reinforced high strength concrete composite shear walls with different steel fiber volume fractions. *Eng. Struct.* **2018**, *171*, 247–259. [[CrossRef](#)]
44. Ministry of Housing and Urban-Rural Development of the People’s Republic of China. *GB 50010-2010 Code for Design of Concrete Structures*; China Building Industry Press: Beijing, China, 2010.

45. Ministry of Housing and Urban-Rural Development of the People's Republic of China and General Administration of Quality Supervision, Inspection and Quarantine of the People's Republic of China. *GB 50936-2014 Technical Specifications for Concrete Filled Steel Tubular Structures*; China Building Industry Press: Beijing, China, 2014.
46. Vetr, M.G.; Shirali, N.M.; Ghamari, A. Seismic resistance of hybrid shear wall (HSW) systems. *J. Constr. Steel Res.* **2016**, *116*, 247–270. [[CrossRef](#)]
47. China Ministry of Construction. *Standard for Evaluation of Concrete Compressive Strength. GB/T 50107–2010*; China Ministry of Construction: Beijing, China, 2010.
48. China Ministry of Construction. *Test Methods of Steel for Reinforcement of Concrete. GB/T 28900–2012*; China Ministry of Construction: Beijing, China, 2012.
49. Liang, X.; Li, J. *GB/T 228-2002, Metallic Materials—Tensile Testing at Ambient Temperature*; China Architecture & Building Press: Beijing, China, 2002.
50. Liao, F. *Study on Seismic Behavior of Reinforced Concrete Shear Walls with Concrete-Filled Steel Tubular Side Columns.*; Fuzhou University: Fuzhou, China, 2007.
51. Jiuru, T.; Chaobin, H.; Kaijian, Y.; Yongcheng, Y. Seismic behavior and shear strength of framed joint using steel–fiber reinforced concrete. *J. Struct. Eng.* **1992**, *118*, 341–358. [[CrossRef](#)]